RESEARCH ARTICLE

Identification Method for Pulse Wave Resulted From Fault Transient of Overhead Transmission Line

YUE YU[1], LONGHAO LIU[1], ZEXIN ZHOU[1], (Senior Member, IEEE), ZHANPENG DU[2], AND CHONGQING JIAO [2]

[1]State Key Laboratory of Power Grid Safety, Relay Protection Research Department, China Electric Power Research Institute, Beijing 100192, China
[2]School of Electrical and Electronic Engineering, North China Electric Power University, Beijing 102206, China

Corresponding author: Chongqing Jiao (cqjiao@ncepu.edu.cn)

ABSTRACT This paper presents a simple and effective method to extract the identification quantity of transient pulse waveform produced by the overhead transmission line short-circuit fault. This method employs the second-order time harmonic equation of the power frequency component to convert the fault full-wave data. After the conversion, only the identification quantity remains. This method can amplify high-frequency spectral content by the times of the square of the angular frequency, and hence improve the sensitivity of identifying fault transient. Using the identification quantity, one can clearly observe the arrival time and relative intensity of fault transient. A three-phase half wavelength transmission line of 50Hz/3000km is simulated with PSCAD to illuminate the effectiveness of this method. The effects of fault type, soil resistivity, fault resistance, power frequency fluctuation, sampling rate, transposition length, fault inception angle and white noise are analyzed. Calculated results show that this method can distinguish different fault type and can work effectively at low sampling rate down to 10kHz. This method is helpful for improving the performance of the traveling-wave based fault location method.

INDEX TERMS Fault location, line fault, power transmission line, pulse, traveling wave.

I. INTRODUCTION

During the normal operation of overhead power transmission lines, there are mainly power frequency voltage and current on them. When a fault occurs on the line, there will be not only power frequency components, but also fault components in the voltage and current. The fault component can be understood as the narrow pulse wave propagating from the fault point to both sides of the fault point along the line. Mastering the propagation process and characteristics of the pulse wave are important for traveling-wave-based fault location method introduced in the review papers [1] and the IEEE standard [2]. Especially, in [2] five types of traveling-wave fault locators are described. The performance

The associate editor coordinating the review of this manuscript and approving it for publication was Ehab Elsayed Elattar [ID].

of traveling-wave method had been analyzed for applications in real 500kV ac transmission lines [3], distribution systems [4], cable lines [5], and high-voltage dc transmission systems [6], [7].

The traveling-wave location method mainly consists of two steps: the first is determining the arrival time of the fault transient, and the second is to deduce the fault location using the arrival time [7], [8]. This article focuses on the first step. Once the first step is carried out, the second step can refer to the existing results and experience adopted in traveling wave location method, typically including the single-ended [9] and double-ended methods [10]. As aforementioned, they can further be classified into five types.

As well as known, the complete time domain voltage/current waveform resulting from line fault occurring at any point of the transmission line can be obtained

through measurement or simulation. However, the complete fault waveform consists of a load component, steady-state component, and transient component [11]. Among them, only the transient component is sent from the fault point and propagates along both sides of the line. Hence, the transient component is especially suitable for traveling wave-based fault location and diagnosis. Unfortunately, it is usually not easy to separate and iden-tify the transient component (a narrow pulse) from the full shape [12]. For example, in traditional traveling-wave based fault location method, to identify the arrival of the fault transient, the sampling rate of the current acquisition system is up to 1 MHz [8], [13], [14], [15], [16]. This greatly limits the applicability of this method.

To relax this limitation, we propose a data processing method to eliminate all power frequency components and meanwhile only remain the transient component. This method employs the second-order time harmonic equation of the power frequency component to convert the full fault waveform. After the conversion, only the identification quantity for fault transient remains. This method can amplify high-frequency spectral content by the times of the square of the angular frequency, and hence improve the sensitivity of identifying fault transient and correspondingly relax the requirement for sampling rate. Through this identification quantity, we can clearly show the prop-agation process of the transient component as a solitary wave on a transmission line. After determining the arrival time, we can use the idea of the existing traveling wave method to apply to single-ended or multi-ended scenarios [2], [17].

Similar to the wavelet transform method [18], [19], [20], the method proposed in this paper also belongs to the traveling wave method in essence. The difference lies in the identification algorithm of the arrival time of the fault traveling wave: the wavelet transform method uses the wavelet transform to extract the high-frequency transient; The method in this paper is not to directly extract the high-frequency transient, but to extract the identifier quantity corresponding to the high-frequency transient. Secondly, in comparison, the algorithm in this paper is simpler, and it is only used to identify the arrival time of the fault transient, and the information that can be extracted is limited; The wavelet method algorithm is more complex, but by selecting different wavelet functions, more local and refined time and frequency domain information can be extracted. The method in this paper has the advantages of simplicity, and may be used as an optional method. In addition, this method can amplify the high-frequency components of a signal, so it has better sensitivity to fault transients and can work at a lower sampling rate.

If this method is compared with other fault location methods (except traveling-wave method), the conclusion of comparison between traveling-wave method and other methods can be directly used. These conclusions have been included in Table 1 and Table 2 of Ref. [21]. In addition, the proposed method will be compared with

TABLE 1. Comparison between the present method and Conventional traveling wave method.

Method	Conventional traveling-wave method	The present method
Sampling frequency	>100kHz	>10kHz
Accuracy	0.1%-0.7%	0.74%-0.90%
network	Single, double, and multi-terminal	Similar to the left
System	AC, DC	Similar to the left
Operational speed	Very fast (0.1-1ms)	Similar to the left
Cost of equipment	high	Similar to the left or less
Algorithm for extracting the arrival time	Complex	simple
Noise robustness	medium	Similar to the left

TABLE 2. Influence of the inception angle on the arrival time.

Fault type	Inception angle	Error (%)
A-g	0°	0.74
	30°	0.76
	45°	0.74
	60°	0.74
	90°	0.76
A-B	0°	0.74
	30°	0.74
	45°	0.90
	60°	0.90
	90°	0.82

the traditional traveling wave method as shown in Table 1. It can be seen that the proposed method has advantages in simplicity and low sampling rate. In other projects, this method is basically similar to the traditional traveling wave method.

The limitations of this method are similar to those of traditional traveling wave methods [20], including: 1) high sampling rate requirements and high equipment cost; 2) the accuracy of traveling wave fault location depends on a proper determination of wave velocity in the transmission line, which may vary with the changes in ambient temperature, icing and dirt on phase conductors. 3) Synchronization of fault locators installed on both ends of transmission line is realized through the use of a GPS. The time synchronization error is estimated to be 1μs, which is equal to ±150m error of determining fault location for a single fault locator.

This paper also verifies the effectiveness of this method by the case analysis conducted in the PSCAD simulation for a 50Hz/3000km half wavelength power transmission line. This method is expected to be useful in traveling-wave-based fault location methods for long-distance ac lines, dc lines, and half wavelength lines. Theoretically, this method is applicable

to any case where a pulse signal superimposes on a lower-frequency time-harmonic signal. For example, it can also be used to identify transient waves in other scenarios, such as the interference of substation switching transients on secondary cables [22], [23].

The rest of this paper is organized as follows. In Section II, the pulse identification quantity extraction method is presented. In Section III, we introduce a simple analytical case based on a lossless and well matched two-wire line. Section IV describes the model of a three-phase 50Hz half wavelength transmission line. Section V contains some basic results for different fault types. Section VI discusses some influence factor like soil resistivity, fault resistance, frequency fluctuation sampling rate, transposition length, fault inception angle and white noise. Finally, Section VII concludes this paper.

II. THE PULSE IDENTIFICATION QUANTITY EXTRACTION METHOD

As is well known, any time-harmonic function $f(t)$ with an angular frequency ω_0 satisfies the following equation:

$$\frac{\mathrm{d}^2 f}{\mathrm{d}t^2} + \omega_0^2 f = 0 \tag{1}$$

For the current waveform $i(t)$ recorded at any observation point after the transmission line fault, its evolution with time can be divided into three stages:

Stage 1: it is a time-harmonic function of time with angular frequency ω_0 when $t > t_1$.

Stage 2: It is a non-sinusoidal waveform when $t_1 < t < t_2$.

Stage 3: it is the other time-harmonic function of time with angular frequency ω_0 when $t > t_2$.

Wherein, ω_0 is actually the power frequency of the transmission line, t_1 represents the time when the fault pulse wavefront first reaches the observation point, and t_2 denotes the time when the fault pulse wave tail leaves the observation point.

The pulse wave identification quantity is defined as:

$$i_{\mathrm{id}} \triangleq \frac{\mathrm{d}^2 i}{\mathrm{d}t^2} + \omega_0^2 i \tag{2}$$

In the following, for simplicity, 'pulse wave identification quantity' is denoted as 'identifier'.

This identifier has the unit of A/s^2. For voltage waves, the corresponding identifier may also be defined in a similar way. Considering that current signal is usually employed for relay protection, here we mainly treat the current waveform. In frequency domain, the proposed identifier can be expressed as

$$i_{\mathrm{id}} = \left(\omega_0^2 - \omega^2\right) i \tag{3}$$

wherein, ω is the angular frequency of the current waveform. From Equation (3), we can see that the identifier can eliminate the 50Hz base frequency from the observed waveform, and meanwhile amplifies its high-frequency spectral content by the times of the square of the angular frequency. The higher

the frequency, the greater the magnification. From this point of view, this method can improve the sensitivity of identifying fault transient, since a fault transient usually contains lots of high-frequency components.

Substituting the aforementioned three-stage current waveform into Equation (2), one can obtain

$$i_{\mathrm{id}} = \begin{cases} 0, & t < t_1 \\ \text{a transient pulse}, & t_1 < t < t_2 \\ 0, & t > t_2 \end{cases} \tag{4}$$

As shown in Equation (4), the identifier i_{id} only exists for the time range from t_1 to t_2. Beyond this range, it is always zero. Hence, it can simply represent the transient component.

In practice, the full waveform of the current is usually measured with a current transformer and is recorded as discrete data. For this reason, we should use the difference operation to approximate the differential operation. With this approximation, Equation (2) can be converted into

$$i_{\mathrm{id}} \triangleq (t) \frac{i(t+\Delta t) + i(t-\Delta t) - 2i(t)}{(\Delta t)^2} + \omega_0^2 i(t) \tag{5}$$

wherein, Δt is the sampling time step. That is, the reciprocal of the sampling rate. Figure 1 displays an intuitive graphical explanation for the three-stage current waveform $i(t)$ and the extraction of its identifier i_{id}.
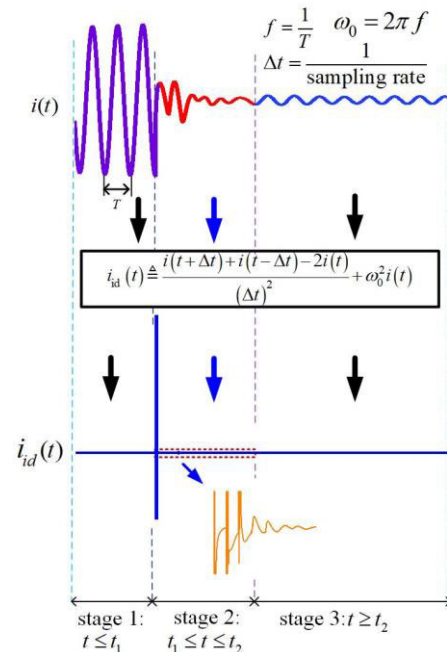

FIGURE 1. Evolution of the three-stage current waveform i(t) and its identifier i_{id} (t).

III. A SIMPLE ANALYTICAL CASE: A LOSSLESS AND MATCHED TWO-WIRE LINE

Figure 2 shows a two-wire line. The line will always be drawn parallel to the z axis. At the sending end ($z = 0$),
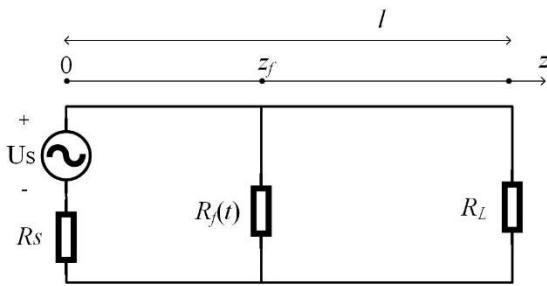
FIGURE 2. A lossless, two-wire transmission line $R_f(t)$ denotes the fault resistance.

the source is represented as a time-harmonic voltage u_s with a source resistance R_S. At the receiving end ($z = l$), the load is represented as a resistance R_L. Wherein, l is the line length.

The line is assumed to be uniform and lossless with characteristic impedance Z_c and phase constant β. Assuming the line is completely matched ($R_s = R_L = Z_c$) and $u_s = u_0 \cos \omega t$, the line current and voltage can be written as

$$u(z, t) = \frac{1}{2} u_0 \cos(\omega_0 t - \beta z) \tag{6a}$$

$$i(z, t) = \frac{1}{2Z_c} u_0 \cos(\omega_0 t - \beta z) \tag{6b}$$

The two are pure traveling waves in the $+z$ direction.

When a fault occurs, a transient wave will send out from the fault point. Here, the fault is modelled as a fault resistance R_f, which is connected to the line as a parallel element as shown in Figure 2. It is assumed that the fault occurs at the time $t = t_0$ and the position $z = z_f$. The fault resistance is described as

$$R_f = \begin{cases} \infty, & t \leq t_0 \\ f(t), & t_0 \leq t \leq t_0 + t_f \\ R_{fs}, & t \geq t_0 + t_f \end{cases} \tag{7}$$

For $t < t_0$, it is infinite since no fault happens before t_0. For $t_0 < t < t_0 + t_f$, it is time varying. For $t > t_0 + t_f$, it is stable at a fixed value of R_{fs}. Wherein, t_f denotes the duration of the dynamic evolution of the fault resistance.

On the right side of the fault point, the transient pulse comes from the refraction of the incident wave and propagates along the $+z$ direction [24]. Its voltage and current can be expressed as, respectively

$$u_{\text{right}}(z, t) = \frac{R_f}{2R_f + Z_c} u_0 \cos[\omega_0 t - \beta z],$$
$$t_0 + t_d \leq t \leq t_0 + t_f + t_d \tag{8a}$$

$$i_{\text{right}}(z, t) = \frac{R_f}{2R_f + Z_c} \frac{1}{Z_c} u_0 \cos[\omega_0 t - \beta z],$$
$$t_0 + t_d \leq t \leq t_0 + t_f + t_d \tag{8b}$$

where, t_d is the wave traveling time from the fault position to the observation point and can be calculated by $t_d = (z - z_f)/c$ with c being the wave speed.

On the left side of the fault point, the transient pulse comes from the reflection of the incident wave and propagates along the $-z$ direction [24]. Its voltage and current can be expressed as, respectively

$$u_{\text{left}}(z, t) = \frac{-Z_c}{2R_f + Z_c} \frac{u_0}{2} \cos[\omega_0 t + \beta z - 2\beta z_f],$$
$$t_0 + t_d \leq t \leq t_0 + t_f + t_d \tag{9a}$$

$$i_{\text{left}}(z, t) = \frac{1}{2R_f + Z_c} \frac{u_0}{2} \cos[\omega_0 t + \beta z - 2\beta z_f],$$
$$t_0 + t_d \leq t \leq t_0 + t_f + t_d \tag{9b}$$

where, t_d is calculated by $t_d = (z_f - z)/c$. The total voltage on the left side is the sum of the incident voltage with the reflected voltage, which is equal to the voltage on the right side (u_{right}). Hence, the voltage continuity can be satisfied.

Substituting Equation (8b) into Equation (1), we obtain the identifier for $z > z_f$ like

$$i_{d,\text{right}} = \frac{u_0}{Z_c} \left[\cos(\omega_0 t - \beta z) \frac{\mathrm{d}^2}{\mathrm{d}t^2} \left(\frac{R_f}{2R_f + Z_c} \right) - 2\omega_0 \sin(\omega_0 t - \beta z) \frac{\mathrm{d}}{\mathrm{d}t} \left(\frac{R_f}{2R_f + Z_c} \right) \right] \tag{10}$$

Similarly, the identifier for $z < z_f$ is

$$i_{d,\text{left}} = \frac{u_0}{2} \left[\cos(\omega_0 t + \beta z - 2\beta z_f) \frac{\mathrm{d}^2}{\mathrm{d}t^2} \left(\frac{1}{2R_f + Z_c} \right) - 2\omega_0 \sin(\omega_0 t + \beta z - 2\beta z_f) \frac{\mathrm{d}}{\mathrm{d}t} \left(\frac{1}{2R_f + Z_c} \right) \right] \tag{11}$$

It can be seen that the identifier depends on the time-varying characteristic of the fault resistance, the characteristic impedance of the line, and the phase of incident wave at fault time.

The above model is very simple due to the assumptions of both complete impedance match and lossless line. Its advantage is to provide us an analytical example to illustrate the proposed identification method. In practice, the impedances are usually not matched with the line. Also, the line is usually lossy. For a lossless line, even if the impedances are not matched, an analytical solution are still available, noting that there will be both forward and backward traveling waves simultaneously before the fault occurrence. However, for a lossy line, considering the propagation constant is frequency-dependent, analytical solutions are unavailable [24]. Hence, in the following, for an overhead three-phase ac transmission lines, we use PSCAD software to numerically simulate the wave process. It should also be noted that, realistically, the behavior of R_f versus time t is usually very difficult to be determined accurately. However, this does not affect the applicability of the proposed pulse extraction method, since the current data can be measured directly in practice.
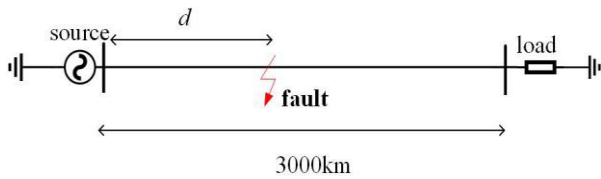
FIGURE 3. A 50Hz/3000km half wavelength power transmission line with a line fault occurring at the position with a distance d from the sending end.
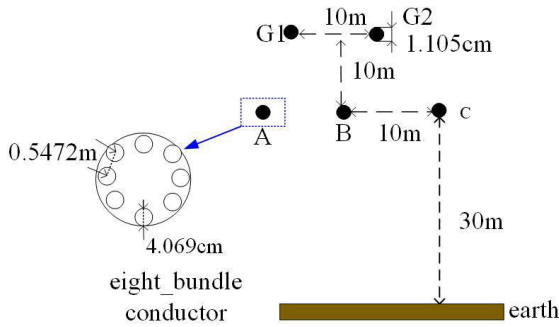

FIGURE 4. Geometrical parameters of the simulated transmission line.

IV. THE TRANSMISSION LINE MODEL

Usually, since the traveling wave fault location method is more suitable for long-distance transmission lines, a 50Hz/3000 km half wavelength power transmission line are employed, as shown in Figure 3. Wherein, a line fault occurs at the position with a distance d from the sending end. The voltage of the sending end is fixed at 400kV. Figure 4 show the tower configuration of this transmission line. The dc resistance is 0.0321Ω/km and 2.8645Ω/km for phase wire and ground wire, respectively. The transposition length is about 100km. In this paper, this transmission line is first modelled as a perfectly transposed line, and then in section VI-E, the impact of the transposition length on the identifier is investigated. At power frequency 50Hz, the positive sequence impedance is 0.034+j0.42 Ω/km, and the positive sequence admittance is j2.74μS/km; the zero sequence impedance is 0.29+j1.16Ω/km, and the zero sequence admittance is j1.88μS/km. It is assumed that the fault occurs at $t_0 = 0.2114$s. In practice, the duration time of fault evolution (t_f) varies from case to case. For wire-to-wire short circuit, this time is on the order of air discharge and may be as short as tens of nanoseconds [25]. On the other hand, for wire-to-earth fault with high impedance, the time will be relatively much longer. Here, we build a frequency-dependent phase-domain transmission line model in PSCAD to simulate the line fault. The time step in PSCAD simulation is always 1μs. Since in PSCAD simulation the short circuit is accomplished with one time-step by default, the corresponding time t_f is about 1μs. In theory, smaller t_f is also considered. However, its lower limit is restricted since transmission line model is based on the quasi-TEM (transverse electromagnetic) wave assumption [24]. This assumption requires that the transverse

dimensions of the line should be electrically small. For a transient with $t_f = 100$ns, the corresponding high frequency component may be up to 3-10MHz, and hence the wavelength may be smaller than 30-100m, which will violate the electrically-small dimension condition. On the other hand, the attenuation constant is frequency-dependent. That is, the higher the frequency, the greater the attenuation constant. Hence, with the increase of the propagation distance, the high-frequency components of a transient waveform will become more and more negligible, compared to the low-frequency components. Also, a transient pulse will undergo waveform distortion and its width will increase. That is, the rising portion of the waveforms becomes less steep. For example, the measured results for a 500kV line shows that the rise time of is about 1.8μs when the observation point is 89km far from the fault point. Wherein, the transient waveforms are detected at the sampling rate of 40MS/s. Considering the above two reasons, we use $t_f = 1$μs in our PSCAD simulations.

Usually, current signals are employed for catching fault transient. Also, the phase currents are decomposed into a ground and two aerial modes with reference to phase A using Clarke's transformation [26] as in the following equation:

$$\begin{bmatrix} I_0 \\ I_\alpha \\ I_\beta \end{bmatrix} = \frac{1}{3} \begin{bmatrix} 1 & 1 & 1 \\ 2 & -1 & -1 \\ 0 & \sqrt{3} & -\sqrt{3} \end{bmatrix} \begin{bmatrix} I_a \\ I_b \\ I_c \end{bmatrix} \qquad (12)$$

where I_0 is the ground mode component and I_α(alpha), I_β (beta) are the aerial mode components. The ground mode has heavier attenuation than the aerial modes, due to more losses in the earth [17]. In addition, the uncertainty of soil resistivity makes it difficult to determine the attenuation coefficient of ground model. As a result, only aerial modes are suitable for analyzing fault characteristics [27]. It should be noted, although the zero, alpha and beta modes can be useful as a 0th order approximation, they are not propagation modes of actual single-circuit overhead lines [28]. However, the error is usually negligibly small for frequency above 500 Hz [28]. As a result, they can be employed with good accuracy since the proposed identifier is mainly determined by the high-frequency components of fault transient.

For convenience, Figure 5 shows the flowchart for extraction of the identifier from current data produced by PSCAD simulation.

V. SOME BASIC RESULTS
A. THE RECEIVING END IS OPEN
1) THE PHASE A TO GROUND FAULT
With a soil resistivity of 100Ω·m, a fault resistance of 10Ω, and a phase A to a ground fault occurring at the midpoint of the line ($d = 1500$km), Figure 6 shows the current waveforms of the ground, alpha and beta modes at the sending end, including both the full wave and the pulse wave identification quantity.
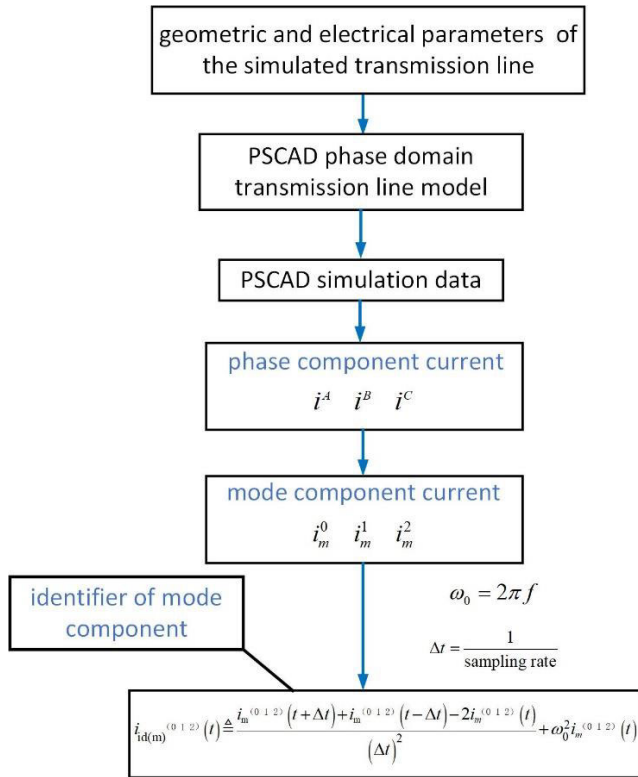
FIGURE 5. The flowchart for extraction of the identifier from current data produced by PSCAD simulation.
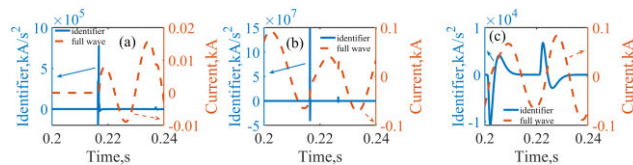

FIGURE 6. The current waveforms of both full wave and identifier at the sending end when a phase A to ground fault occurs at the midpoint of the transmission line with open load: (a) the ground mode I_0, (b) the alpha mode $I\alpha$ and (c) the beta mode I_β.

It can be seen that the identifier appears at the time of $t = 0.2164$s, which is a 5ms delay from the time of fault occurrence ($t_0 = 0.2114$s). This pulse identification wave corresponds to the first traveling-wave arrival. This time delay is exactly the time required for an electromagnetic wave to travel the 1500km distance from the fault point to sending end. In addition, a smaller pulse identification wave can also be observed at $t = 0.2264$s for ground and alpha modes, which corresponds to the second traveling-wave arrival. It has a time delay of 15ms and a 4500km propagation path. As shown in Figure 7, the 4500km path may correspond to two cases: (1) first from the fault point to the receiving end (1500 km), and then from the receiving end to the sending end (3000km); (2) first from the fault point to the sending end (1500km), second from the sending end the fault point (1500km), and finally again from the fault point to the sending end (1500km).
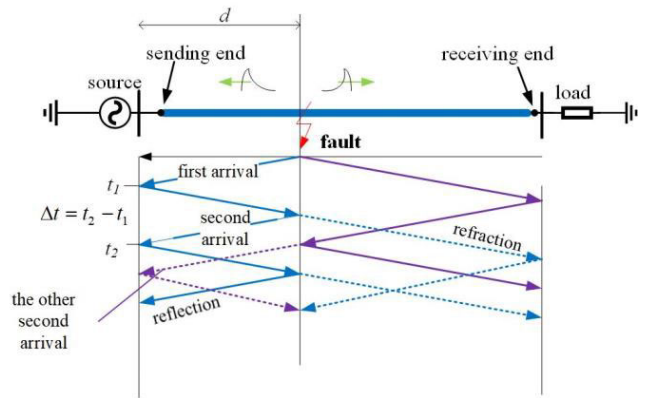

FIGURE 7. Lattice diagram showing the reflections and refractions caused by the traveling waves when a fault is present on a power system.

It can also be clearly seen that the identifier only appears at the time range when the transient component of the full wave is passing the observation point. Also, the identifier for the alpha mode is much larger than that for the ground mode. Meanwhile, the identifier for the ground mode is also much larger that for the beta mode. Hence, the phase A to ground fault can be identified when the alpha mode has much larger identifier than the other two modes.
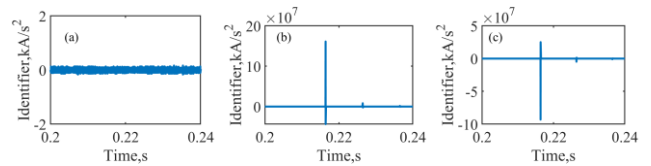

FIGURE 8. The waveform of identifier at the sending end when a phase A to phase B fault occurs at the midpoint of the transmission line with open load: (a) the ground mode I_0, (b) the alpha mode I_α and (c) the beta mode I_β.

2) THE PHASE A TO PHASE B FAULT

With a phase A to phase B fault occurring at the same position, Figure 8 shows the identifier waveforms of the ground, alpha and beta modes at the sending end. In this case, the identifier for the ground mode is much smaller than the other two modes. The identifier for the beta mode is about half of that for the alpha mode. Hence, the phase A to phase B fault can be identified when the identifier for alpha mode is the largest and the identifier for ground mode is relatively much smaller.
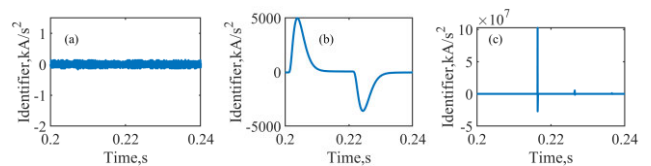

FIGURE 9. The waveform of identifier at the sending end when a phase B to phase C fault occurs at the midpoint of the transmission line with open load: (a) the ground mode I_0, (b) the alpha mode I_α and (c) the beta mode I_β.

3) THE PHASE B TO PHASE C FAULT

With a phase B to phase C fault occurring at the same position, Figure 9 shows the identifier waveforms of the ground, alpha and beta modes at the sending end. In this case, the identifier for the beta mode is much larger than the alpha mode. And the identifier for the alpha mode is also much larger than that for the ground mode. Hence, the phase B to phase C fault can be identified when the identifier for beta mode is further greater than these for the other two modes.
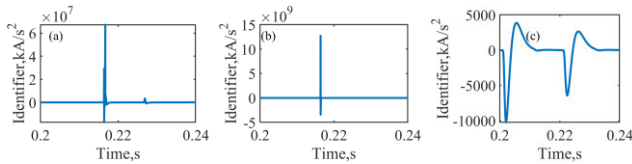

FIGURE 10. The waveform of identifier at the sending end when a phase A to ground fault occurs at the midpoint of the transmission line with matched load: (a) the ground mode I_0, (b) the alpha mode I_α and (c) the beta mode I_β.

B. THE RECEIVING END IS MATCHED

1) THE PHASE A TO GROUND FAULT

Figure 10 shows the identifier waveforms of the ground, alpha and beta modes at the sending end for phase A to ground fault with matched load. A comparison between Figure 6 and Figure 10 illuminates that the previous conclusion for identifying phase A to ground fault in case of open load is also suitable for the present case of matched load.
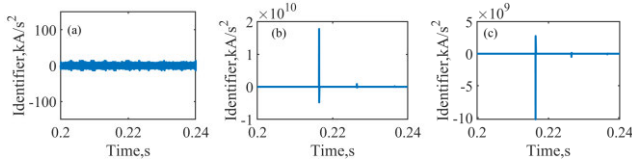

FIGURE 11. The waveform of pulse wave identification at the sending end when a phase A to phase B fault occurs at the midpoint of the transmission line with matched load: (a) the ground mode I_0, (b) the alpha mode I_α and (c) the beta mode I_β.

2) THE PHASE A TO PHASE B FAULT

Figure 11 shows the identifier waveforms of the ground, alpha and beta modes at the sending end for phase A to phase B fault with matched load. A comparison between Figure 8 and Figure 11 illuminates that the previous conclusion for identifying phase A to phase B fault in case of open load is also suitable for the present case of matched load.

3) THE PHASE B TO PHASE C FAULT

Figure 12 shows the identifier waveforms of the ground, alpha and beta modes at the sending end for phase B to phase C fault with matched load. A comparison between Figure 9 and Figure 12 illuminates that the previous conclusion for identifying phase B to phase C fault in case of open load is also suitable for the present case of matched load.
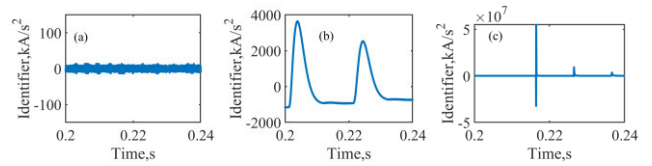

FIGURE 12. The waveform of identifier at the sending end when a phase A to phase B fault occurs at the midpoint of the transmission line with matched load: (a) the ground mode I_0, (b) the alpha mode I_α and (c) the beta mode I_β.

VI. DISCUSSIONS ON SOME INFLUENCE FACTOR

In this section, for simplicity and without loss of generality, we mainly employ the phase A to ground fault with matched load to investigate the effects of soil resistivity, fault resistance, frequency fluctuation, and sampling rate on the identifier. Also, in most cases, we only show the identifier for alpha mode, considering that it is much larger than the ground mode and the beta mode.

A. THE SOIL RESISTIVITY

In practice, soil resistivity is affected by factors such as soil components, structure and humidity, and can vary with location and time [29], [30], [31]. A rain can significantly reduce the soil resistivity. Usually, soil resistivity can vary from tens of Ω·m to thousands of Ω·m.
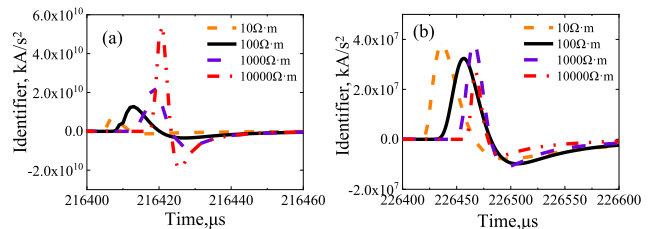

FIGURE 13. The waveform of the first arrival (a) and second arrival (b) of the alpha mode identifier at the sending end when a phase A to ground fault occurs at the midpoint of the transmission line with matched load. Different soil resistivities are considered: 10Ω·m(orange line), 100Ω·m(black line), 1000Ω·m(purple line), and 10000Ω·m (red line).

With a fault resistance of 10Ω, Figure 13 plot the identifier for the alpha modes: Figure 13(a) and Figure 13(b) correspond to the first and second arrival respectively. Figure 13(a) shows that the peak of the identifier of the first arrival rises with the resistivity increasing. Meanwhile, the arrival time will delay with the soil resistivity increasing, which can be attributed to the faster propagation speed for lower soil resistivity. According to Figure 13(b), the peak of the identifier of the second arrival no longer changes monotonously with the increase of soil resistivity. Similar to the first arrival, the second arrival will also delay with the soil resistivity increasing. The time difference between the first and second arrivals is approximately equal for the four kinds of soil resistivity.

B. THE FAULT RESISTANCE

In practice, fault resistance can be affected by factors like fault type and surface contact. Usually, fault resistance can vary from several ohms to thousands of ohms [32], [33]. With a soil resistivity of 100Ω·m, Figure 14 plot the identifier for the alpha modes. This figure shows that the identifier decreases with the fault resistance increasing. The ratio of identifier peak is about 13: 9.3: 2.5, when the fault resistance is in the order of 10Ω, 100Ω and 1000Ω. In term of peak arrival time, the three curves are in good agreement.
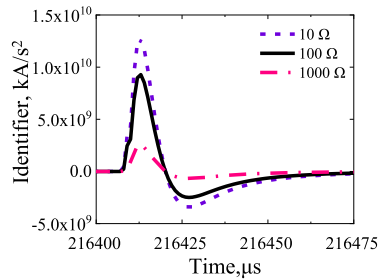

FIGURE 14. The waveform of alpha mode at the sending end when a phase A to ground fault occurs at the midpoint of the transmission line with matched load for different fault resistances: 10Ω(purple line), 100Ω(black line) and 1000Ω(red line).
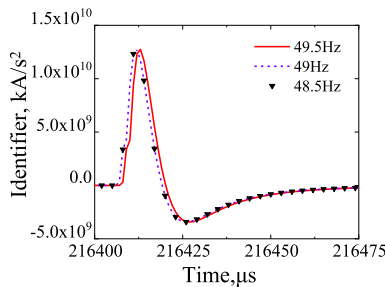

FIGURE 15. The waveform of alpha mode at the sending end when a phase A to ground fault occurs at the midpoint of the transmission line with matched load for different frequency fluctuation: -0.5 Hz (49.5Hz), -1 Hz (49Hz) and-1.5 Hz (48.5Hz).

C. THE FREQUENCY FLUCTUATION

In practice, the power frequency may have tiny fluctuation around the its ideal value (50Hz). For example, the frequency deviation for power system in China is usually less than ±0.2Hz [34]. Here, to investigate the influence of frequency fluctuation, we assume that the frequency used to extract the pulse quantity is always maintained at 50Hz, but the power frequency used in PSCAD simulations fluctuates around it. Calculated results of alpha mode are shown in Figure 15 for −0.5Hz, −1Hz and −1.5Hz frequency deviation from the standard 50Hz, respectively. Wherein, the soil resistivity is 100Ω·m and the fault resistance is 10Ω. It can be seen that the identifier is hardly affected by this tiny frequency fluctuation.
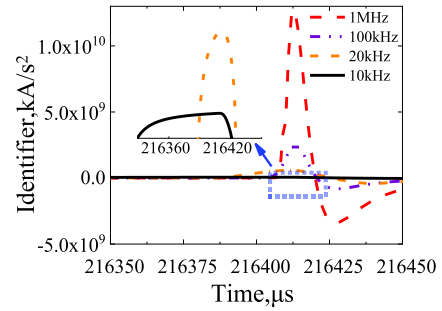

FIGURE 16. The waveform of alpha mode at the sending end when a phase A to ground fault occurs at the midpoint of the transmission line with matched load for different sampling rate: 1MHz (red line), 100kHz (purple line), 20kHz (orange line), and 10kHz (black line).

D. THE SAMPLING RATE

In practice, the current signal is detected by a current transformer. Usually, current transformers have narrow bandwidth (typically less than 10-50kHz). Correspondingly, the downstream data acquisition device also works at low sampling rate. High sampling rate up to 1MHz can cause heavy burden on improving present current transformers, in term of bandwidth expansion and mass data storage. Here, we investigate the effect of sampling rate on the identifier waveform, as shown in Figure 16. Wherein, the sampling rate is reduced from 1MHz to 100kHz, 20kHz and 10kHz, respectively. Correspondingly, the time step Δt used in Equation (5) is increased from 1μs to 10μs, 50μs and 100μs, respectively. The soil resistivity is 100Ω·m and the fault resistance is 10Ω. We can see that, although its peak value decreases rapidly with the decrease of the sampling rate, the time when the peak value appears almost remains unchanged. In this sense, the proposed identifier can work at low sampling rate like 10kHz. If the sampling rate is further reduced to 5kHz, the agreement of peak arrival time will deteriorate (the corresponding curve is not provided, since it is very flat with no obvious peak). As a result, a sampling rate below 5kHz is not acceptable.
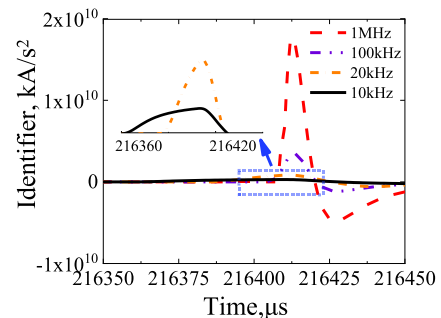

FIGURE 17. The waveform of alpha mode at the sending end when a phase A to phase B fault occurs at the midpoint of the transmission line with matched load for different sampling rate: 1MHz (red line), 100kHz (purple line), 20kHz (orange line), and 10kHz (black line).

FIGURE 18. The waveform of beta mode at the sending end when a phase B to phase C fault occurs at the midpoint of the transmission line with matched load for different sampling rate: 1MHz (red line), 100kHz (purple line), 20kHz (orange line), and10kHz (black line).
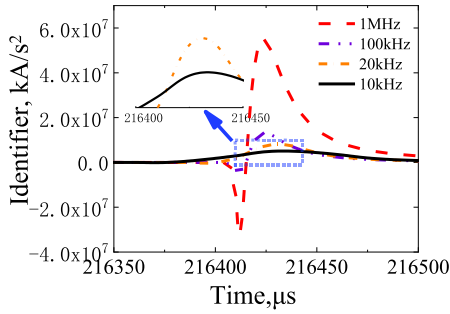
Further, Figure 17 displays the corresponding results for alpha mode in case of phase A to phase B fault. And Figure 18 illuminates the corresponding results for beta mode in case of phase B to phase C fault. We can see from the two figures that 10kHz sampling rate is also feasible for the two types of faults.

E. TRANSPOSITION LENGTH

As aforementioned, this actual transposition length is about 100km. According to Ref.35, a single-circuit overhead line can exhibit repetitive resonant behaviour at frequencies such that the overall transposition cycle length gets close to an integer multiple of one half wavelength. As a result, the proposed identifiers may be interfered by these high-frequency resonance effects. To address this concern, calculated results for two kinds of transposition length (50km, 100km) are plotted in Figs. 19-21 for A-ground, A-B, and B-C faults, respectively. Wherein, the soil resistivity is $100\Omega\cdot m$, the fault resistance is 10Ω, the sampling rate is 1MHz, and the load is matched.

It can be seen that, there are some extra small pulses after the first pulse. The time interval between the neighbored small pulses is about twice the time of wave propagation through a transposition segment. It is $670\mu s$ and $335\mu s$, for 100km and 50km transposition length, respectively. This agrees with the resonance behaviour in [35]. The magnitude of the first pulse is much larger than that of the following pulses. Meanwhile, the arrival time of the first pulse is same to that in the case of the above perfectly transposed line. In this sense, employing the first pulse, the interference caused by the resonance effects can be neglected.

It should also be emphasized that, compared with the results of the perfectly transposed line in Section V, the order of the relative magnitudes of the identifier for the modes has changed. For example, in A-ground fault, the beta mode is now the largest, but alpha mode is also close to it; In A-B fault, the beta mode is the largest and meanwhile is much larger than alpha mode; In A-C fault, the alpha mode is the largest, but beta mode is close to it. In contrast, for the perfectly transposed line, in A-ground fault the alpha mode is the largest and is much larger than the beta mode; In
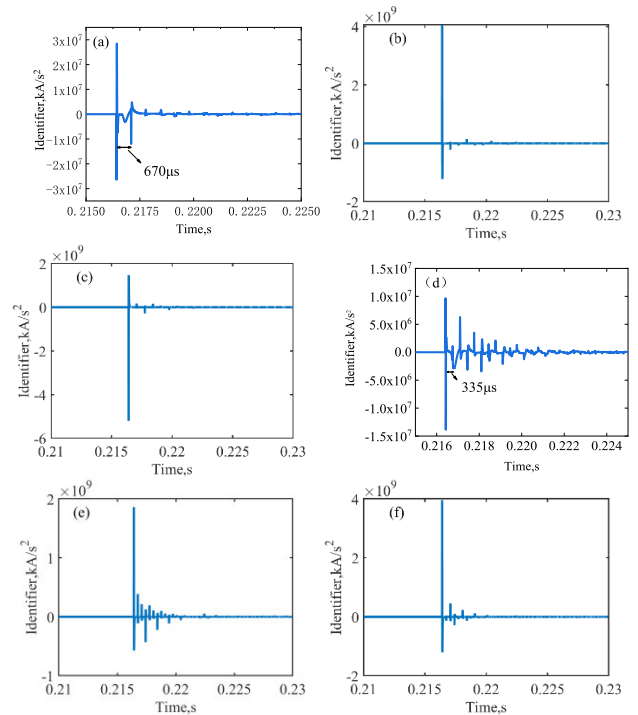

FIGURE 19. The waveform of identifier at the sending end when a phase A to ground fault occurs at the midpoint of the transmission line with matched load: (a) the ground mode I_0 with transposition length of 100km, (b) the the alpha mode I_α with transposition length of 100km, (c) the beta mode I_β with transposition length of 100km, (d) the ground mode I_0 with transposition length of 50km, (e) the alpha mode I_α with transposition length of 50km and (f) the beta mode I_β with transposition length of 50km.

A-B fault, the alpha mode is the largest but the beta mode is also close to it; In A-C faults, the beta mode is the largest and is also much larger than the alpha mode. Therefore, the conclusion of how to predict the fault type from the relative magnitudes of the identifiers is greatly affected by the transposition length. Here, the considered transmission line is very long, which may complicate the role of transposition length.

F. FAULT INCEPTION ANGLE

In Ref.8 and Ref.17, the fault inception angle was considered in term of its effect on the arrival time of fault traveling wave. Here, we consider it from a similar way. Especially, with different inception angles, we calculated the corresponding propagation time $\Delta t'$, which is defined as the difference between the time when the peak of the identifier reaches the observation point and the time when the fault occurs. Meanwhile, the theoretical value of propagation time (Δt) is calculated with $\Delta t = \Delta L /v$. Wherein, ΔL is the distance from the fault position to the observation point at the sending end, and v is the velocity of the fault traveling wave. The wave velocity v for aerial mode usually varies from 2.95×10^5 km/s to 3×10^5 km/s [20], [36]. Here, we select the value of 2.97×10^5 km/s. Finally, the accuracy of determining the arrival time by using the proposed identifier is measured by
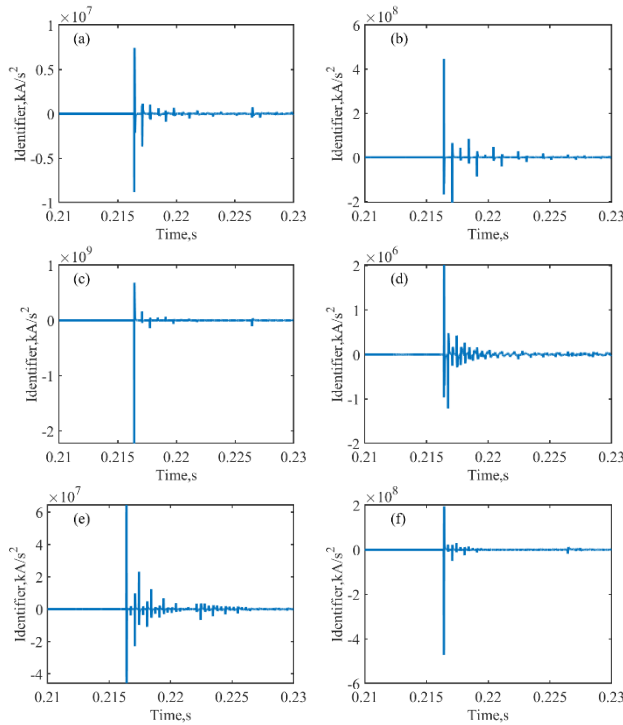
FIGURE 20. The waveform of pulse wave identification at the sending end when a phase A to phase B fault occurs at the midpoint of the transmission line with matched load: (a) the ground mode I_0 with transposition length of 100km, (b) the alpha mode I_α with transposition length of 100km, (c) the beta mode I_β with transposition length of 100km, (d) the ground mode I_0 with transposition length of 50km, (e) the alpha mode I_α with transposition length of 50km and (f) the beta mode I_β with transposition length of 50km.

the following relative error of Equation (13).

$$\text{error} = \frac{|\Delta t - \Delta t'|}{\Delta t} \quad (13)$$

For different inception angles, the error is calculated for both phase A to ground and phase A to phase B faults. The adopted soil resistivity is 100Ω·m and the fault resistance of 10Ω. The results are shown in the table 2. It can be seen that the error is between 0.74% - 0.90%, and the effect of inception angle on the error is negligible. It should be noted, the error can be reduced to 0.18%-0.26% further if the velocity is increased to 3×10^5 km/s. However, the practical velocity of alpha mode is slighted affected by many factors and is difficult to be accurately determined. Sometimes, measurement for practical transmission lines is necessary to find the exact value of the velocity.

G. IMPACT OF WHITE NOISE

In Ref.17, noise is investigated in term of its effect on the arrival time difference of modal traveling waves. Especially, the noise is a Gaussian white noise and is added to the modal traveling wave signal. The adopted signal-to-noise ratio (SNR) is 80dB, 85dB, 90dB, 95dB, and 100dB, respectively. Here, the effect of Gaussian white noise under different SNR (80dB, 85dB, 90dB, 95dB, 100dB) on the identifier of alpha

mode is calculated for the phase A to ground fault with the soil resistivity of 100Ω·m and the fault resistance of 10Ω. The results show that the higher the SNR, the smaller the impact of noise.
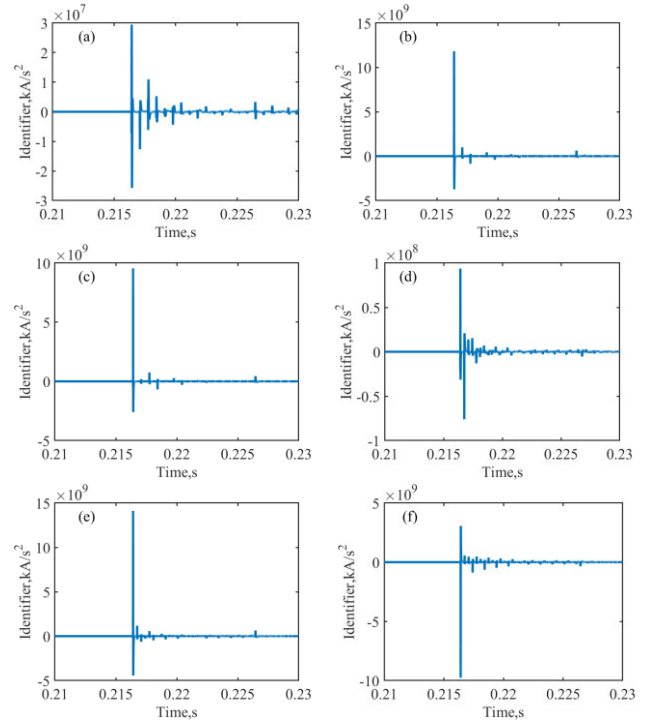

FIGURE 21. The waveform of identifier at the sending end when a phase B to phase C fault occurs at the midpoint of the transmission line with matched load: (a) the ground mode I_0 with transposition length of 100km, (b) the alpha mode I_α with transposition length of 100km, (c) the beta mode I_β with transposition length of 100km, (d) the ground mode I_0 with transposition length of 50km, (e) the alpha mode I_α with transposition length of 50km and (f) the beta mode I_β with transposition length of 50km.
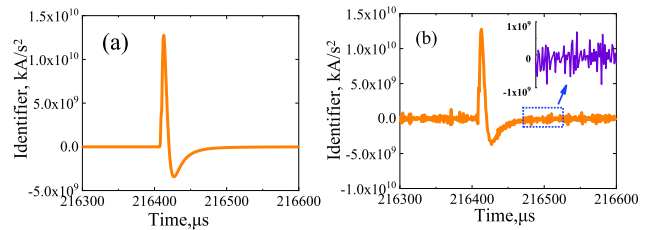

FIGURE 22. The identifier of alpha mode for the phase A to ground fault with the soil resistivity of 100Ω·m and the fault resistance of 10Ω. (a) the noise is zero, (b) a Gaussian white noise with SNR=80dB.

The worst-case results for the SNR of 80dB is shown in Figure 22(b), meanwhile, in Figure 22(a), the result with zero noise is also provided for comparison. It can be seen that the noise can cause the identifier to be non-zero all the time. However, the contribution of the noise to the identifier is less than 10^9kA/s^2 and is much smaller than the peak (about 1.2×10^{10}kA/s^2) of the identifier of the fault transient. Hence, the effect of the noise is negligible.

VII. CONCLUSION

By substituting the full fault waveform data into the second-order time harmonic equation of power frequency, the power frequency component can be easily eliminated, and only the identifier generated by the fault transient can be retained. Theoretically, this method is applicable to any case where a pulse signal superimposes on a lower-frequency time-harmonic signal. Primarily, this method is employed to the traveling-wave based on protection of transmission lines to identify the arrival time and relative intensity of the transient resulted from short-circuit fault. Then, the fault position and type can also be evaluated. Simulated results for the perfectly-transposed half-wavelength line show that, the identifier decreases with the increase of the fault resistance and with the decrease of the soil resistivity, but hardly affected by the frequency fluctuation. By comparing the relative intensity of the three identifiers for ground, alpha and beta modes, different fault types can be distinguished. This method has the advantages of improving the sensitive of identifying transient component by amplifies its high-frequency spectral content by the times of the square of the angular frequency. Also, it can work at lower sampling rate like 10kHz. By contrast, traditional traveling-wave location method requires the sampling rate up to 1MHz. Compared with wavelet and other methods, the algorithm in this paper is simpler, so it can be used as an alternative method.

It should be noted that, the present results are preliminary. Lots of influence factor have not been considered like different fault locations, lines with different voltage levels, the line length and type, the time evolution behavior of the fault resistance, and the transposition length. The feasibility of this method applied to complex transmission line configuration like ring network and complex fault type like indirect lighting needs to be analyzed. Especially, as shown in section VI-E, the finite transposition length can cause resonance effect at some special frequencies and leads to different rule to distinguish fault types, compared with the perfect transposition. In addition, the comprehensive positioning error analysis and the corresponding experimental validation are desirable. All these issues are reserved for future research.

REFERENCES

[1] K. Chen, C. Huang, and J. He, "Fault detection, classification and location for transmission lines and distribution systems: A review on the methods," *High Voltage*, vol. 1, no. 1, pp. 25–33, Apr. 2016.

[2] *IEEE Guide for Determining Fault Location on AC Transmission and Distribution Lines*, Standard C37.114-2014, Revision of IEEE Std C37.114-2004, Jan. 2015, pp. 1–76.

[3] C. Zhuang, S. Xie, H. Yang, H. Yu, Y. Geng, and R. Zeng, "Flexible noncontact approach for fault location of transmission lines using electro-optic field sensors," *IEEE Trans. Electromagn. Compat.*, vol. 63, no. 6, pp. 2151–2158, Dec. 2021.

[4] R. Chen, X. Yin, X. Yin, Y. Li, and J. Lin, "Computational fault time difference-based fault location method for branched power distribution networks," *IEEE Access*, vol. 7, pp. 181972–181982, 2019.

[5] M. Zhang, K. Zhao, Y. Yan, Y. Lu, S. Yang, L. Wang, and H. Li, "A double-terminal traveling-wave-based method using novel noncontact sensors for fault location in transmission cable lines," *IEEE Access*, vol. 9, pp. 80797–80805, 2021.

[6] Q. Huai, L. Qin, K. Liu, H. Ding, X. Liao, and T. Tan, "Combined line fault location method for MMC–HVDC transmission systems," *IEEE Access*, vol. 8, pp. 170794–170806, 2020.

[7] C. Zhang, G. Song, and X. Dong, "A novel traveling wave protection method for DC transmission lines using current fitting," *IEEE Trans. Power Del.*, vol. 35, no. 6, pp. 2980–2991, Dec. 2020.

[8] O. D. Naidu and A. K. Pradhan, "Precise traveling wave-based transmission line fault location method using single-ended data," *IEEE Trans. Ind. Informat.*, vol. 17, no. 8, pp. 5197–5207, Aug. 2021.

[9] C. Zhang, G. Song, T. Wang, and L. Yang, "Single-ended traveling wave fault location method in DC transmission line based on wave front information," *IEEE Trans. Power Del.*, vol. 34, no. 5, pp. 2028–2038, Oct. 2019.

[10] F. V. Lopes, P. Lima, J. P. G. Ribeiro, T. R. Honorato, K. M. Silva, E. J. S. Leite, W. L. A. Neves, and G. Rocha, "Practical methodology for two-terminal traveling wave-based fault location eliminating the need for line parameters and time synchronization," *IEEE Trans. Power Del.*, vol. 34, no. 6, pp. 2123–2134, Dec. 2019.

[11] L. Fu, Z. He, and Z. Bo, "Novel approach to fault classification in EHV transmission line based on multi-information measurements of fault transients," in *Proc. Asia–Pacific Power Energy Eng. Conf.*, Mar. 2009, pp. 1–4.

[12] X. Lin, F. Zhao, G. Wu, Z. Li, and H. Weng, "Universal wavefront positioning correction method on traveling-wave-based fault-location algorithms," *IEEE Trans. Power Del.*, vol. 27, no. 3, pp. 1601–1610, Jul. 2012.

[13] H. Shu, X. Liu, and X. Tian, "Single-ended fault location for hybrid feeders based on characteristic distribution of traveling wave along a line," *IEEE Trans. Power Del.*, vol. 36, no. 1, pp. 339–350, Feb. 2021.

[14] T. A. H. Mustafa, D. W. P. Thomas, C. Christopoulos, and A. Raizer, "Comparison of simulated and recorded transients for travelling wave fault location," in *Proc. IEEE Bologna Power Tech. Conf.*, Jun. 2003, p. 4.

[15] *Ultra-High-Speed Line Relay, SEL-T401L*. [Online]. Available: https://selinc.com/products/T401L/

[16] S. Marx, "Traveling wave fault location in protective relays: Design, testing, and results," in *Proc. 6th Annu. Georgia Tech Fault Disturbance Anal. Conf.*, Atlanta, GA, USA, May 2013, pp. 68–81.

[17] R. Liang, N. Peng, L. Zhou, X. Meng, Y. Hu, Y. Shen, and X. Xue, "Fault location method in power network by applying accurate information of arrival time differences of modal traveling waves," *IEEE Trans. Ind. Informat.*, vol. 16, no. 5, pp. 3124–3132, May 2020.

[18] K. Buthelezi, M. Kabeya, and M. Leoaneka, "A review of fault location algorithms utilising travelling wave, wavelet transform and multi-resolution analysis techniques," in *Proc. 30th Southern Afr. Universities Power Eng. Conf. (SAUPEC)*, Jan. 2022, pp. 1–6.

[19] C. Subramani, A. A. Jimoh, M. Sudheesh, and I. E. Davidson, "Fault investigation methods on power transmission line: A comparative study," in *Proc. IEEE PES PowerAfrica*, Jun. 2016, pp. 93–97.

[20] G. Krzysztof, R. Kowalik, D. Rasolomampionona, and S. Anwar, "Traveling wave fault location in power transmission systems: An overview," *J. Electr. Syst.*, vol. 7, no. 3, pp. 287–296, 2011.

[21] H. Panahi, R. Zamani, M. Sanaye-Pasand, and H. Mehrjerdi, "Advances in transmission network fault location in modern power systems: Review, outlook and future works," *IEEE Access*, vol. 9, pp. 158599–158615, 2021.

[22] H.-T. Wu, X. Cui, X.-F. Liu, C.-Q. Jiao, R. Hu, W.-J. Chen, and L. Wang, "Characteristics of electromagnetic disturbance for intelligent component due to switching operations via a 1100 kV AC GIS test circuit," *IEEE Trans. Power Del.*, vol. 32, no. 5, pp. 2228–2237, Oct. 2017.

[23] H. Wu, C. Jiao, X. Cui, X. Liu, and J. Ji, "Transient electromagnetic disturbance induced on the ports of intelligent component of electronic instrument transformer due to switching operations in 500 kV GIS substations," *IEEE Access*, vol. 5, pp. 5104–5112, 2017.

[24] C. R. Paul, *Analysis of Multiconductor Transmission Lines*, 2nd ed. Hoboken, NJ, USA: Wiley, 2008.

[25] D. M. Xiao, *Gas Discharge and Gas Insulation*. Shanghai, China: Shanghai Jiaotong Univ. Press, 2017.

[26] E. Clarke, "*Circuit analysis of AC power systems. Symmetrical and Related Components*. Hoboken, NJ, USA: Wiley, 1943.

[27] E. O. Schweitzer, A. Guzman, M. V. Mynam, V. Skendzic, B. Kasztenny, and S. Marx, "Locating faults by the traveling waves they launch," in *Proc. 67th Annu. Conf. Protective Relay Engineers*, Mar. 2014, pp. 95–110.

[28] J. A. B. Faria, "Application of Clarke's transformation to the modal analysis of asymmetrical single-circuit three-phase line configurations," *Eur. Trans. Electr. Power*, vol. 10, no. 4, pp. 225–231, Sep. 2007.

[29] J. He, B. Zhang, and R. Zeng, "Maximum limit of allowable ground potential rise of substation grounding system," *IEEE Trans. Ind. Appl.*, vol. 51, no. 6, pp. 5010–5016, Nov. 2015.

[30] B. Zhang, Y. Jiang, J. Wu, and J. He, "Influence of potential difference within large grounding grid on fault current division factor," *IEEE Trans. Power Del.*, vol. 29, no. 4, pp. 1752–1759, Aug. 2014.

[31] M. G. Unde and B. E. Kushare, "Impact of seasonal variation of soil resistivity on safety of substation grounding system," in *Proc. 5th Int. Conf. Adv. Recent Technol. Commun. Comput. (ARTCom)*, 2013, pp. 173–182.

[32] J. An, C. Zhuang, F. Rachidi, and R. Zeng, "An effective EMTR-based high-impedance fault location method for transmission lines," *IEEE Trans. Electromagn. Compat.*, vol. 63, no. 1, pp. 268–276, Feb. 2021.

[33] J. Sun, Q. Yang, W. Xu, and W. He, "A distribution line fault location estimation algorithm based on electromagnetic time-reversal method calculated in the finite difference time domain," *IEEE Trans. Electromagn. Compat.*, vol. 64, no. 3, pp. 865–873, Jun. 2022.

[34] *National Standard of the People's Republic of China*, document GB/T 15945-2008, Power quality-Frequency Deviation for Power System.

[35] J. A. B. Faria and M. V. Guerreiro das Neves, "Nonuniform three-phase power lines: Resonance effects due to conductor transposition," *Int. J. Electr. Power Energy Syst.*, vol. 26, no. 2, pp. 103–110, Feb. 2004.

[36] C. M. S. Ribeiro, F. V. Lopes, and K. M. Silva, "Assessment of traveling wave propagation velocity on HVDC transmission lines," in *Proc. Workshop Commun. Netw. Power Syst. (WCNPS)*, Nov. 2022, pp. 1–6.

LONGHAO LIU received the M.Eng. degree in electrical engineering from The University of Melbourne, Australia, in 2016.

He is currently with China Electric Power Research Institute. His research interests include fault characteristics and protection technology of power systems.

ZEXIN ZHOU (Senior Member, IEEE) was born in Fujian, China, in 1969. She is currently with the Protection Relay Department, China Electric Power Research Institute, Beijing, China. Her research interest includes power system protection.

ZHANPENG DU is currently pursuing the degree in electrical engineering with North China Electric Power University, Beijing, China. His main research interests include spatial electromagnetic disturbance characteristics and suppression measures under switching operation of substations.

YUE YU received the M.A. degree in electrical engineering and automation from North China Electric Power University, Beijing, China, in 2010. She is currently with China Electric Power Research Institute. Her research interests include fault characteristics and protection technology of power systems.

CHONGQING JIAO received the B.Sc. degree in geophysics from the Chinese University of Geosciences, Wuhan, China, in 2002, and the Ph.D. degree in physical electronics from the Institute of Electronics, Chinese Academy of Sciences, Beijing, China, in 2007. He is currently an Associate Professor of electrical and electronic engineering with North China Electric Power University, Beijing. His research interests include electromagnetic theory and applications, and the EMC in power systems.

● ● ●